Available online at www.easd.procedia.org
EASD Procedia EURODYN (2026) 2475-2486

EASD Procedia

EURODYN 2026
XIII International Conference on Structural Dynamics
M. Beer, C. Papadimitriou, H. Jensen, J. Chen, M. Broggi, J. Behrensdorf (eds.)
Hannover, Germany, 27.09.–01.10 2026

MULTI-CLASS VIBRATION EVENT CLASSIFICATION IN A MONITORED HERITAGE STEEL–GLASS HALL

Aliasghar Talebi[1], **Marianna Crognale**[1], **and Vincenzo Gattulli**[1]

[1]Department of Structural and Geotechnical Engineering
Sapienza University of Rome, Italy
e-mail: {aliasghar.talebi, marianna.crognale, vincenzo.gattulli}@uniroma1.it

Keywords: Structural health monitoring, Blast detection, Physics-informed ML, Synthetic data, Heritage structures, Event classification

Abstract. *On 4 July 2025, a liquefied petroleum gas (LPG) explosion occurred at a petrol station located 6.4 km from the Marcus Aurelius Exedra Hall in Rome. The semi-elliptical steel–glass pavilion, equipped with a permanent accelerometric monitoring system, captured the resulting ground shock across multiple sensors. This study investigates the recorded response through a combined analysis of wave propagation, structural filtering, and multi-class event discrimination under real monitoring conditions. The measured signals show a short-duration impulsive transient followed by a rapidly decaying tail, clearly distinguishable from longer-duration environmental excitations such as thunderstorms. To support physical interpretation, a finite element model calibrated from ambient vibration data is used to compare measured and simulated responses. A feature-based calibration procedure aligns key statistical and spectral descriptors of synthetic excitation signals with measured response characteristics, including RMS amplitude, dominant frequency content, band energy distribution, and peak-related features. For event classification, two complementary machine learning branches are developed: a lightweight 1D-CNN trained on real monitored data, and a physics-informed XGBoost classifier trained exclusively on calibrated synthetic structural responses using response-derived statistical, spectral, and temporal ratio descriptors. A hybrid z-score anomaly detector bridges the synthetic-to-real domain gap, enabling deployment on unlabeled field recordings. The XGBoost classifier achieves 90% window-level accuracy on synthetic test validation, while the hybrid z-score–XGBoost framework successfully identifies a confirmed blast event and a thunderstorm episode on real data, demonstrating the practical transferability of the physics-informed training strategy.*

ISSN:2311-9020 © 2026 The Authors. Published by EASD Procedia.
Peer-review under responsibility of the Organizing Committee of EURODYN 2026.
doi: 10.47964/1326.10843.575

1 INTRODUCTION

Structural Health Monitoring (SHM) systems enable continuous observation of structural response under operational and environmental loading conditions. However, the interpretation of rare, high-energy transient events remains challenging, especially when the source is located at significant distance from the monitored structure. In such cases, the recorded response is modified by attenuation and scattering during propagation, interaction with the built environment [1, 2], and by local site effects and structural filtering [3]. As a result, physically meaningful impulsive events may be difficult to distinguish from environmental excitations such as thunderstorms or operational disturbances. Real-field recordings of blast-like events at structural scale are also limited, and their characterization under realistic monitoring conditions is still not fully understood.

Model-based SHM methods traditionally interpret structural condition through changes in modal parameters such as natural frequencies, damping ratios, and mode shapes [4–8], and their applicability under real monitoring conditions has been demonstrated in field studies [9]. In parallel, data-driven methods rely on signal processing, statistical indicators, and machine learning to extract discriminative information directly from measurements [10, 11]. Their use has expanded with dense monitoring systems and digital twin frameworks [12], and recent studies have shown the effectiveness of convolutional neural networks for vibration-based anomaly detection and event classification under noisy conditions [13]. In previous work by the authors, a CNN-based classifier was integrated into a digital twin framework for the identification of blast-like events in monitored data [14]; related studies have also addressed rare-event detection and class imbalance issues in SHM [15, 16]. Nevertheless, the separation of source-related effects from structural response, together with the need for physically consistent synthetic data, remains an open issue.

In this context, the present study investigates the dynamic response of a heritage steel–glass structure subjected to a remote blast transient, with emphasis on physics-informed synthetic data generation and multi-class event classification. A simplified finite element model calibrated from ambient vibration data supports the generation of synthetic structural responses, while a feature-based calibration procedure aligns synthetic descriptors with measured sensor statistics. The analysis is grounded in a unique full-scale dataset from the Marcus Aurelius Exedra Hall in Rome, recorded during a confirmed LPG explosion in July 2025. A hybrid z-score–XGBoost framework is introduced for deployment on unlabeled real data. Together with the 1D-CNN branch of [14], this forms a dual-branch SHM architecture for reliable multi-class event discrimination under realistic monitoring conditions.

2 INSTRUMENTED SYSTEM AND TRANSIENT EVENT DATASET

The Marcus Aurelius Exedra Hall is a steel–glass pavilion located at the Capitoline Museums in Rome. The structure features a semi-elliptical geometry and is equipped with a permanent Structural Health Monitoring (SHM) system composed of six triaxial MEMS accelerometers [17]. The sensors are installed on three representative columns, with measurements collected at both base and top levels, enabling observation of both local and global structural response. The spatial configuration of the monitoring network allows capturing not only the amplitude of the structural response but also its distribution across the structure, which is particularly relevant for transient events where propagation-related characteristics and structural response patterns may vary across sensor locations.

The monitoring system has been operating continuously for several years, providing an ex-

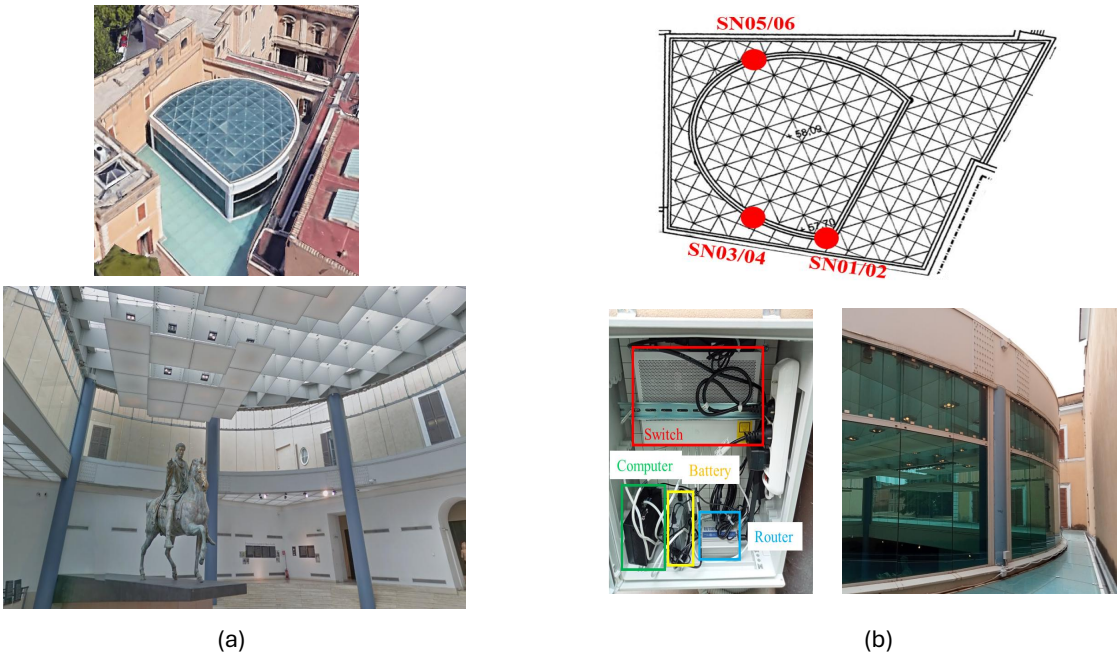


Figure 1: The Marcus Aurelius Exedra Hall at the Capitoline Museums, Rome: (a) aerial and interior views of the steel–glass pavilion, and (b) sensor layout showing the three instrumented column pairs (SN01/02, SN03/04, SN05/06), data acquisition unit, and exterior view of the glass facade.

tensive dataset of ambient, operational, and environmental vibrations. This long-term operation also enables the identification of rare transient events that are not accessible under controlled experimental conditions. On 4 July 2025, a liquefied petroleum gas (LPG) explosion occurred at a petrol station on Via dei Gordiani, approximately 6.4 km from the monitored structure. The event was detected across multiple sensors within a short time interval, appearing as a coherent multi-sensor transient that indicates a common external excitation source. The recorded signals suggest that the excitation propagated predominantly through the ground as a seismic transient, undergoing attenuation and scattering in the urban environment [18], leading to a filtered structural response at the sensor locations. Figure 2 presents representative acceleration signals recorded at sensor SN02 (a_x component) for the blast and thunderstorm events. The two excitations exhibit markedly different temporal and amplitude characteristics. The thunderstorm signal shows a sustained response with a peak acceleration of 0.0338 g, an active duration of approximately 109.78 s, and an SNR of 12.96 dB. In contrast, the blast-induced response is short-duration and impulsive, with a peak of 0.0102 g, an active duration of only 1.41 s, and a higher SNR of 19.41 dB. Despite its lower peak amplitude, the blast signal emerges more clearly above the noise floor, reflecting the concentrated energy release of the impulsive source. These contrasting characteristics motivate the multi-class discrimination framework developed in the following sections. The dataset used in this study includes blast, thunderstorm, and ambient signals collected over extended monitoring periods, providing a suitable basis for both physical interpretation and event classification.

3 SYNTHETIC DATA GENERATION AND MODEL TRAINING

This section presents the generation of synthetic structural responses and their calibration against real measurements to ensure statistical consistency. The calibrated dataset is then used

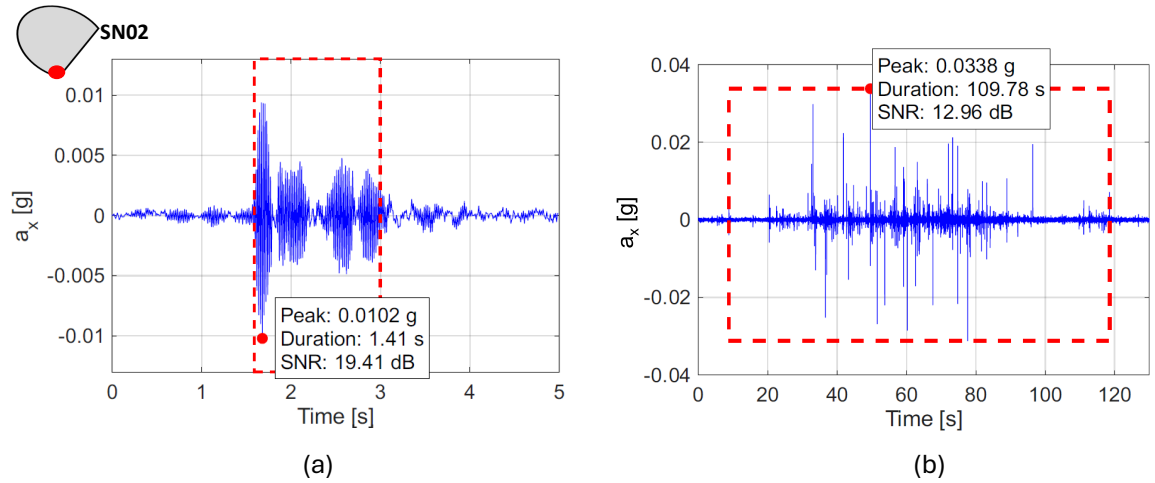


Figure 2: Representative acceleration signals recorded at sensor SN02 (a_x component): (a) blast-induced response (peak: 0.0102 g, duration: 1.41 s, SNR: 19.41 dB), and (b) thunderstorm-induced response (peak: 0.0338 g, duration: 109.78 s, SNR: 12.96 dB), highlighting the contrasting temporal characteristics of impulsive and sustained excitations.

to train a physics-informed XGBoost classifier for multi-class event discrimination.

3.1 Feature-based calibration and synthetic scenario generation

A simplified numerical model of the instrumented structure was developed in OpenSees to generate synthetic acceleration responses under controlled excitation. To improve agreement between simulated and measured responses, a feature-based calibration procedure was introduced at the excitation level using five key descriptors: RMS amplitude, first and second dominant frequencies, band-limited energy ratio, and peak-to-RMS ratio. Denoting by $\mathbf{y}_{\text{real}}$ and $\mathbf{y}_{\text{syn}}(\theta)$ the feature vectors extracted from the measured and synthetic responses, respectively, the calibration problem reads

$$\theta^* = \arg\min_{\theta} \left\| \mathbf{y}_{\text{syn}}(\theta) - \mathbf{y}_{\text{real}} \right\|^2 \tag{1}$$

The calibration results are shown in Fig. 3. Starting from the calibrated baseline, synthetic scenarios were generated by superimposing time-localised perturbations on the background input:

$$u(t) = u_{\text{base}}(t) + u_{\text{event}}(t) \tag{2}$$

Four scenario classes were considered: ambient baseline, hard-negative cases with weak non-event perturbations, impulsive transients with short-duration high-amplitude bursts, and sustained transients with broader temporal extent. Impulsive transients were generated with signal-to-noise ratios in the range 10–16 dB, hard-negative cases with 0–1 dB, and sustained transients with 3–10 dB, ensuring clear separability between classes while maintaining physical plausibility. Amplitude, starting time, duration, and waveform shape were randomized within predefined ranges to ensure variability. All scenarios were generated over 5 s windows and propagated through the numerical model to obtain structurally consistent synthetic responses for the downstream classification framework.

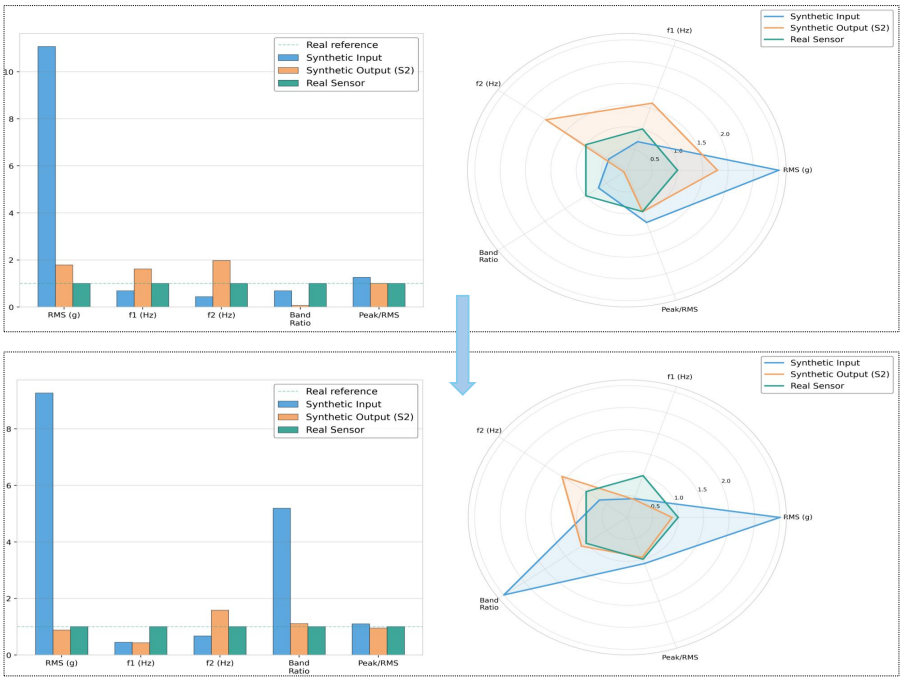


Figure 3: Feature-based calibration of the synthetic ground motion input. Bar charts (left) and radar plots (right) show five features normalized to the real sensor reference before (top) and after (bottom) calibration, demonstrating improved alignment between synthetic structural output and real sensor data in RMS, Peak/RMS, and band ratio.

3.2 Model training framework

The synthetic dataset was organized into 5 s windows and processed using a consistent preprocessing strategy. Two complementary classification branches were defined based on different signal representations. The first branch employs a 1D-CNN applied directly to multichannel response time histories, learning a nonlinear mapping from the input window $\mathbf{X}_i \in \mathbb{R}^{T\times C}$ to class probabilities:

$$\hat{\mathbf{p}}_i = \Psi(\mathbf{X}_i) \tag{3}$$

This branch operates in the time domain without requiring manual feature design and is trained on real monitored data to discriminate between blast, thunderstorm, and ambient events [14]. The second branch uses XGBoost on a reduced physics-informed feature vector combining output-only descriptors and consecutive sub-window ratio features:

$$\mathbf{x}_i = \left[\mathbf{f}_i^{\text{out}},\ \mathbf{f}_i^{\text{ratio}}\right] \tag{4}$$

The output-only features $\mathbf{f}_i^{\text{out}}$ are extracted directly from the structural response signal $y_i(t)$ and include RMS, normalized energy, absolute peak, crest factor, kurtosis, skewness, zero-crossing rate, and exceedance fraction. Input–output ratio features $\mathbf{f}_i^{\text{io}}$ were explored during training to assess the contribution of structural transfer function information, but are not included in the deployment model. They are defined as:

$$f_k^{\text{io}} = \frac{f_k^{\text{out}}}{f_k^{\text{in}} + \varepsilon}, \quad k \in \{\text{RMS},\ \text{energy},\ \text{peak},\ \text{crest}\} \tag{5}$$

where f_k^{in} and f_k^{out} denote the k-th descriptor extracted from the excitation and response signals respectively, and ε is a small regularization constant. Although confirmed to contribute significantly to synthetic validation accuracy, these features were excluded from the final deployment model since the excitation signal is unavailable in real monitoring conditions. Instead, consecutive sub-window ratio features $\mathbf{f}_i^{\text{ratio}}$ are computed over five 1 s sub-windows within each 5 s analysis window to capture temporal evolution without requiring the input signal:

$$f_{k,w}^{\text{ratio}} = \frac{f_{k,w+1}^{\text{out}}}{f_{k,w}^{\text{out}} + \varepsilon}, \quad w = 1, \ldots, 4 \tag{6}$$

where $f_{k,w}^{\text{out}}$ denotes the k-th descriptor of the w-th sub-window. These temporal ratio features encode how each descriptor evolves within the analysis window, capturing the transient onset characteristic of impulsive events. Feature importance analysis on the deployment model confirmed that consecutive sub-window ratio features contribute the largest share of model importance, with energy and kurtosis ratios emerging as the most discriminative descriptors for impulsive event detection. Class probabilities are estimated through a softmax over an additive ensemble of boosted trees, and the predicted class corresponds to the maximum probability output. This branch adopts a four-class taxonomy: ambient, impulsive, sustained, and hard-negative. The hard-negative class represents ambiguous non-event transients and is mapped to ambient in the integrated framework. The two branches remain compatible since their dominant physical behaviours align naturally: ambient corresponds directly across both domains, blast maps to impulsive responses, and thunderstorms map to sustained excitations. A schematic overview of the complete workflow is shown in Fig. 4.

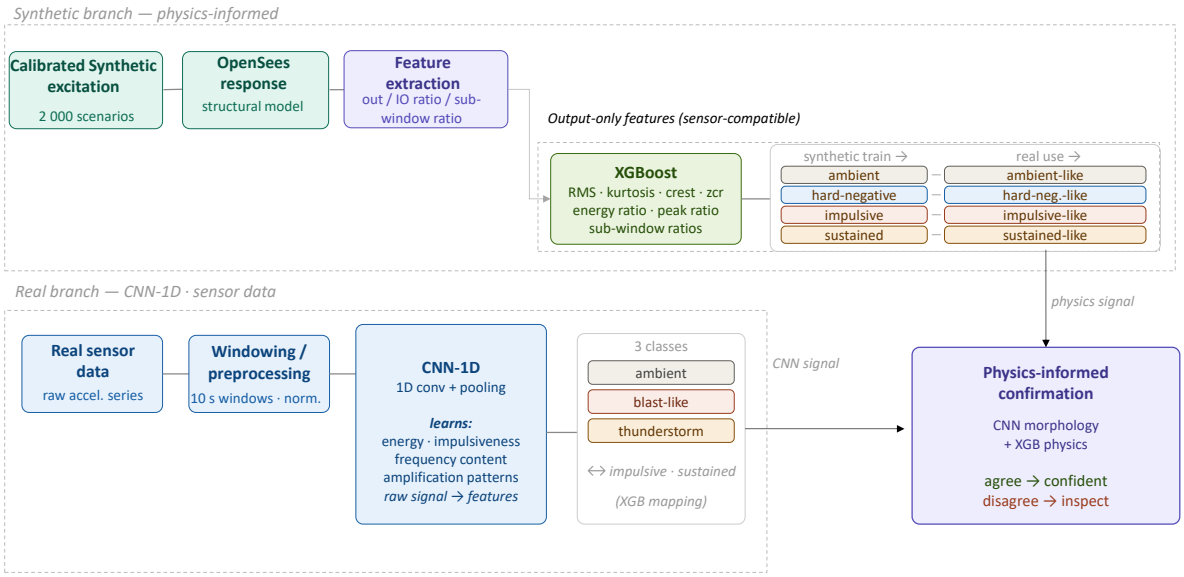


Figure 4: Workflow of the proposed framework: calibrated synthetic input generation, response window extraction, reduced-feature computation, and parallel classification through the physics-informed XGBoost and the 1D-CNN branches.

4 RESULTS

This section presents the main outcomes of the proposed framework, covering synthetic response validation through the physics-informed XGBoost classifier, event discrimination on

real monitored data through the 1D-CNN, and hybrid detection results on confirmed real events.

4.1 Synthetic response validation

Figure 5 shows the XGBoost predictions on a representative 50 s synthetic test signal composed of ten 5 s windows covering all four event classes. The model correctly classifies 9 out of 10 representative test windows, achieving 90% window-level accuracy for this synthetic test sequence. Impulsive events are identified with high confidence (P≥0.89), and ambient windows are consistently classified correctly (P≥0.95). The single misclassification occurs in a sustained window that is predicted as hard-negative (P=0.85), a physically plausible confusion since both classes share similar low-amplitude, broadband characteristics after structural filtering. Crucially, neither sustained nor hard-negative events represent structural damage, so this misclassification would not trigger a false structural alert in practice.

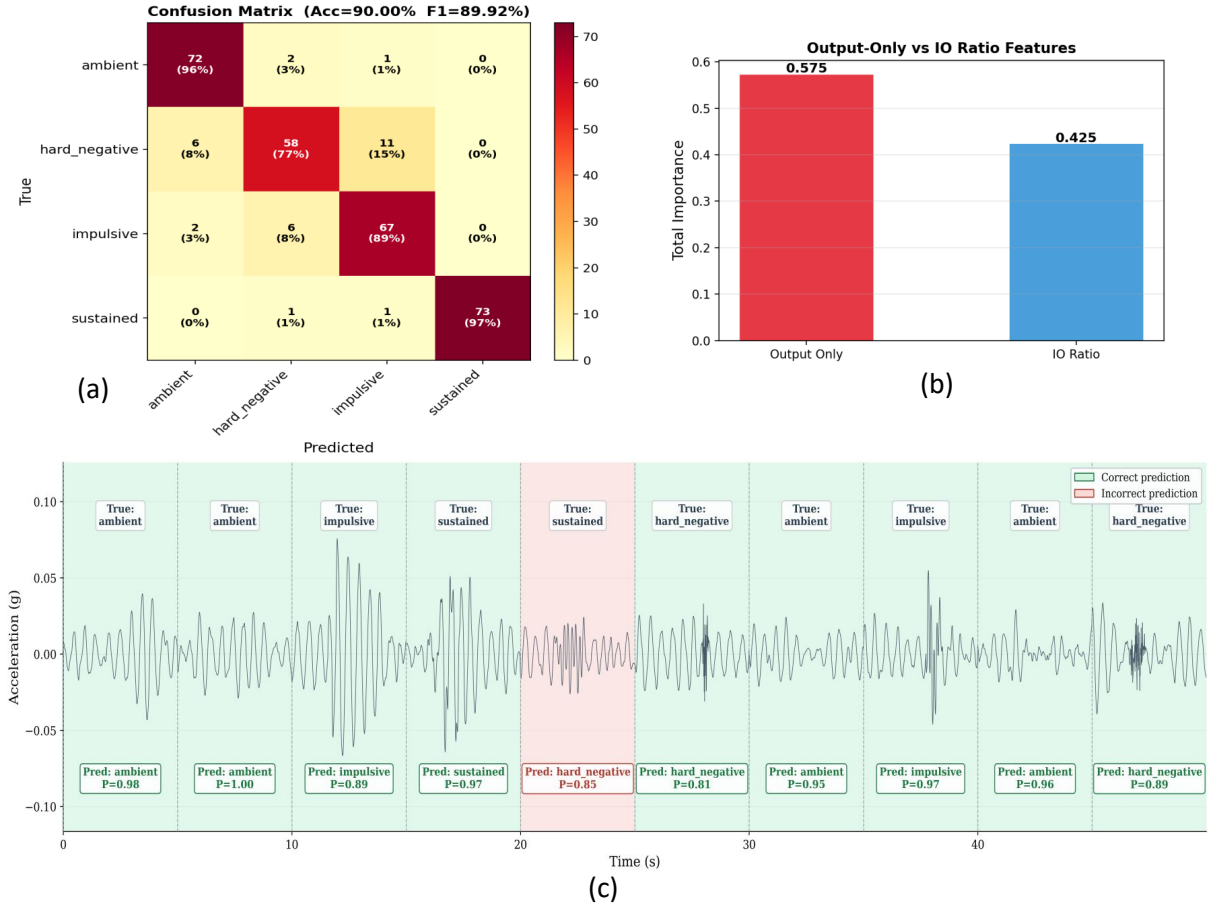


Figure 5: (a) Confusion matrix on the synthetic test set (Acc=90%, Macro F1=89.92%). (b) Total feature importance grouped by output-only and input-output (IO) ratio features for the full synthetic model, showing that IO ratio features contribute 42.5% of model importance despite comprising one third of the feature set. (c) XGBoost predictions on a 50 s synthetic structural response signal covering all four event classes. Green and red boxes indicate correct and incorrect predictions, respectively.

4.2 Event discrimination on real monitored data

The 1D-CNN classifier was evaluated on real monitored data from sensor SN02, covering three event classes: blast, thunderstorm, and ambient. Figure 6 shows the confusion matrix obtained on the test set, summarizing the per-class classification performance. The model demonstrates reliable separation between blast and thunderstorm events, reflecting the distinct temporal characteristics observed in the recorded signals. Ambient windows are correctly identified in the majority of cases, with limited confusion at the boundary with thunderstorm excitations, which is consistent with the gradual onset typical of environmental events.

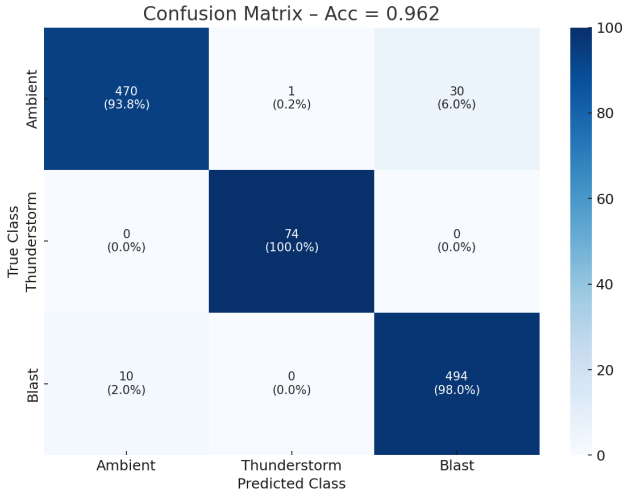


Figure 6: Confusion matrix of the 1D-CNN classifier trained on real labeled data from sensor SN02 (overall accuracy 96.2%). Class-wise accuracies: 93.8% (ambient), 100% (thunderstorm), and 98.0% (blast).

4.3 Physics-informed hybrid detection on real monitored data

The trained XGBoost classifier was applied to real accelerometric data to assess the transferability of the physics-informed training strategy. Since the model was trained exclusively on synthetic structural responses, a hybrid detection framework was adopted to bridge the synthetic-to-real domain gap: a z-score anomaly detector first flags windows exhibiting statistically significant deviations from the ambient baseline using consecutive sub-window feature ratios, while non-anomalous windows are passed to the XGBoost classifier for event type identification. Flagged windows are labeled as impulsive for blast events and sustained for thunderstorm events, based on the physical nature of the excitation.

Figure 7 shows the detection results on a 50-second segment recorded during a confirmed blast event at approximately 08:18 AM on 04/07/2025. Windows W1–W3 (t = 0–15 s) correspond to pre-event ambient conditions and are correctly identified as non-event. Windows W4–W7 (t = 15–35 s) are flagged as impulsive by the anomaly detector, with z-scores ranging from 3.2 to 5.6, driven by sudden increases in the energy ratio between consecutive 1-second sub-windows. The signal returns to ambient in W8–W10, confirming the transient nature of the detected blast.

Figure 8 shows the detection results on a 70-second segment recorded during a confirmed thunderstorm event at approximately 09:40 AM on 28/07/2025. The z-score anomaly detector flags four windows (W4, W6, W7, W8) based on sudden increases in kurtosis between consecutive sub-windows, corresponding to intermittent thunder and rain impact bursts. These flagged

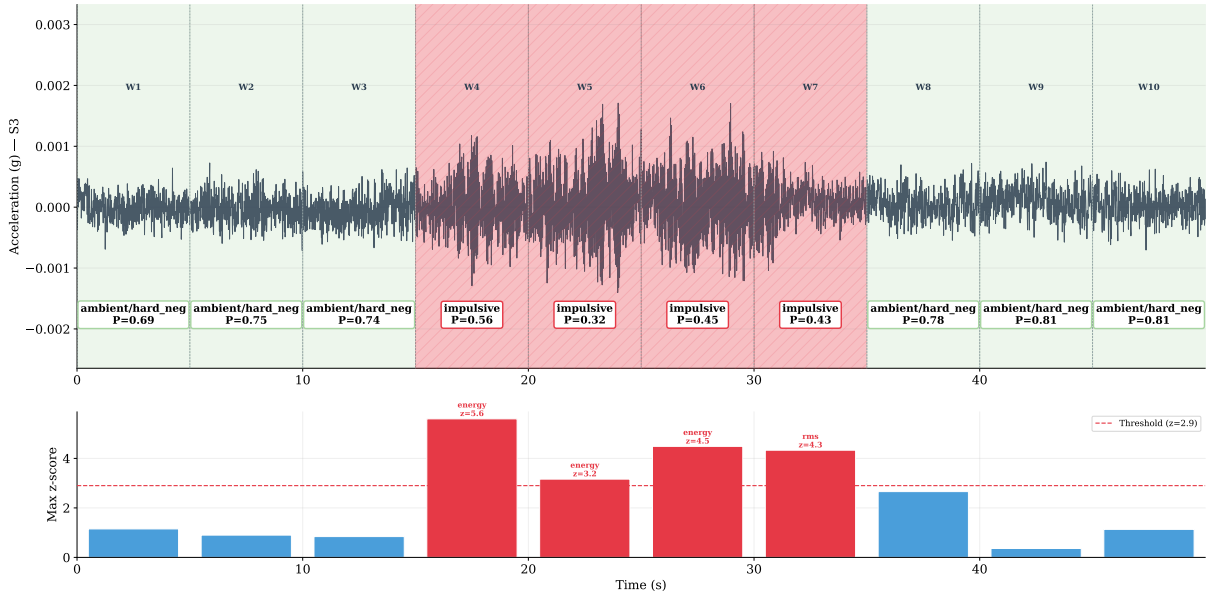


Figure 7: Hybrid XGBoost–z-score detection results for the blast event (04/07/2025, ~08:18 AM). Red hatched regions indicate impulsive windows flagged by the z-score detector (W4–W7, $t \approx 15$–35 s). Lower panel shows the maximum z-score per window; dashed line indicates the detection threshold.

windows are classified as sustained events, consistent with the diffuse and prolonged nature of thunderstorm excitation. The surrounding windows remain below the detection threshold and are correctly identified as ambient conditions, confirming that the framework successfully distinguishes between transient blast excitation — detected through energy ratio anomalies — and sustained weather-induced excitation —detected through kurtosis anomalies.

4.4 Integrated assessment

Table 1 summarizes the classification performance of the two branches across both synthetic and real data, providing a structured basis for comparison.

Branch	Training data	Accuracy	Blast	Thunderstorm
XGBoost (synthetic)*	Synthetic only	90% (synthetic)	Yes	Yes
1D-CNN	Real labeled	96.2% (real)	98.0%	100%

*Hard-negative predictions are mapped to ambient.

Table 1: Classification performance comparison of the two branches.

The results from the three evaluation branches provide consistent and mutually confirming evidence of the framework's effectiveness. The XGBoost classifier, trained exclusively on physics-informed synthetic data, achieved 90% window-level accuracy on the representative synthetic test sequence and successfully detected both a blast and a thunderstorm episode on real unlabeled recordings. The key discriminating features differ between event types: energy ratio anomalies between consecutive sub-windows drive blast detection, while kurtosis anomalies characterize thunderstorm excitation. This physically motivated distinction confirms that the hybrid z-score detector captures event-specific signatures rather than generic amplitude

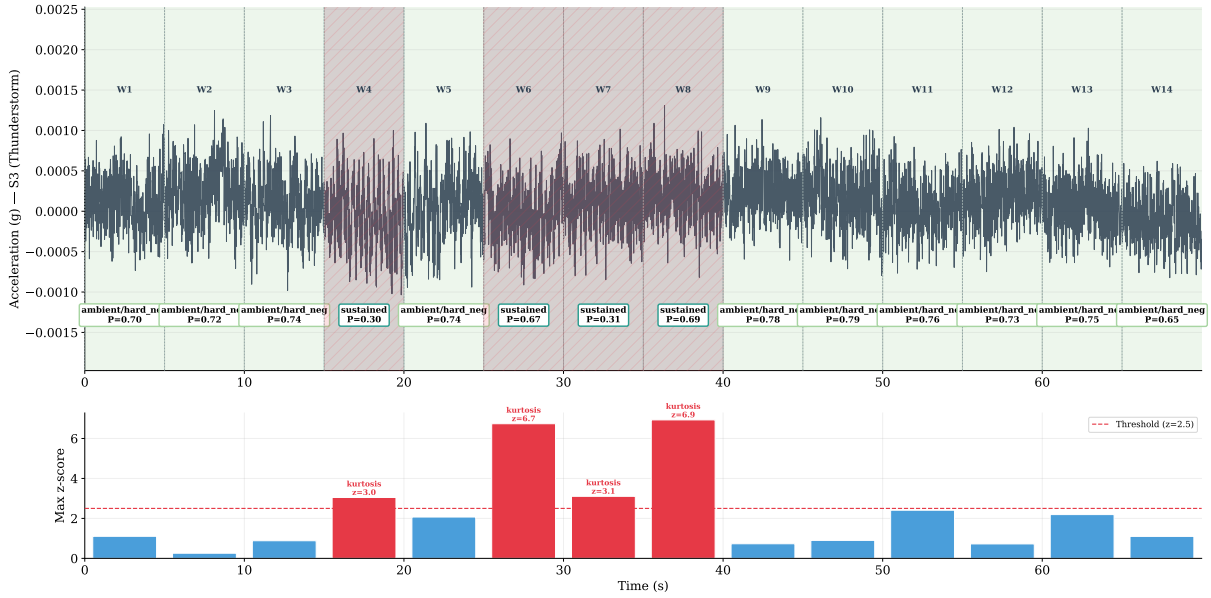


Figure 8: Hybrid XGBoost–z-score detection results for the thunderstorm event (28/07/2025, ~09:40 AM). Sustained excitation is detected in windows W4–W8 ($t \approx 15$–40 s).

thresholds.

The 1D-CNN [14], trained on real labeled data, achieves higher absolute accuracy (96.2%) by exploiting the full waveform morphology. However, it requires annotated real recordings, which are inherently scarce for rare structural events. The XGBoost branch addresses this limitation by relying entirely on synthetic training, at the cost of a moderate accuracy reduction on synthetic data and the need for the z-score bridge on real data.

The two branches are designed to operate jointly in continuous monitoring: the z-score detector flags anomalous windows in real time, which are then independently submitted to both classifiers. When both agree, the classification is accepted with high confidence. When they disagree, the window is flagged for manual review, providing a conservative safety net for rare and potentially damaging events. This dual-branch architecture effectively combines the generalization capability of physics-informed synthetic training with the waveform sensitivity of data-driven learning, offering a practical and robust solution for SHM in data-scarce monitoring scenarios.

5 CONCLUSIONS

This study presented a physics-informed framework for rare-event classification in structural health monitoring, applied to a heritage steel–glass structure subjected to remote blast and thunderstorm excitations. The framework integrates three main components: a feature-based calibration procedure that aligns synthetic ground motion inputs with real sensor response statistics; a physics-informed XGBoost classifier trained on calibrated synthetic structural responses; and a hybrid z-score anomaly detector that bridges the synthetic-to-real domain gap for deployment on unlabeled field data.

The XGBoost classifier achieved 90% window-level accuracy on the representative synthetic test sequence across four event classes. In the exploratory full synthetic model, IO ratio features contributed 42.5% of model importance despite comprising one third of the feature set, confirming the relevance of transfer-related descriptors; however, the deployment model relied

only on response-derived temporal ratio features. When applied to real monitored data, the hybrid z-score–XGBoost detector successfully identified a confirmed blast event (04/07/2025) and a thunderstorm episode (28/07/2025), distinguishing between transient impulsive excitation — flagged through energy ratio anomalies — and sustained weather-induced excitation — flagged through kurtosis anomalies. These results were obtained without any labeled real data, demonstrating the practical value of physics-informed synthetic training for monitoring scenarios where annotated recordings are scarce.

The complementary 1D-CNN branch [14], trained directly on real labeled recordings, achieved 96.2% overall accuracy with 98.0% blast recall and 100% thunderstorm recall. The two branches are designed to operate jointly: agreement between classifiers provides increased confidence in event identification, while disagreement flags windows for manual review, reducing false alerts in continuous monitoring.

Future work will extend the framework to multi-sensor fusion using cross-sensor IO ratio features, investigate few-shot adaptation strategies to fine-tune the XGBoost classifier with a small number of real labeled examples, and assess generalization across multiple monitoring campaigns and structural typologies.

REFERENCES

[1] K. Aki and P.G. Richards. *Quantitative Seismology*. MIT Press, 2002.

[2] M. Kham et al. "Seismic Site–City Interaction: Main Governing Phenomena through Simplified Numerical Models". In: *Bulletin of the Seismological Society of America* 96.5 (2006), pp. 1934–1951.

[3] P.Y. Bard. "Microtremor measurements: a tool for site effect estimation". In: *The Effects of Surface Geology on Seismic Motion*. Vol. 3. 1999, pp. 1251–1279.

[4] S.W. Doebling et al. "Damage identification and health monitoring of structural and mechanical systems from changes in their vibration characteristics: a literature review". In: *Shock and Vibration Digest* 28.2 (1996), pp. 1–25. DOI: 10.2172/249299.

[5] A. Dutta and S. Talukdar. "Damage detection in bridges using accurate modal parameters". In: *Finite Elements in Analysis and Design* 40 (2004), pp. 287–304.

[6] J.J. Moughty and J.R. Casas. "A state of the art review of modal-based damage detection in bridges: development, challenges, and solutions". In: *Applied Sciences* 7.5 (2017), p. 510. DOI: 10.3390/app7050510.

[7] M. Crognale et al. "An integrated vibration-image procedure for damage identification in steel trusses". In: *Proceedings of EURODYN 2020*. 2020, pp. 1011–1018.

[8] M. Crognale, F. Potenza, and V. Gattulli. "Fatigue damage identification by a global-local integrated procedure for truss-like steel bridges". In: *Structural Control and Health Monitoring* (2023). DOI: 10.1155/2023/9594308.

[9] C. Rinaldi et al. "Measured hospital building vibrations induced by air conditioning systems and elevators". In: *Journal of Physics: Conference Series* 2647.14 (2024), p. 142009. DOI: 10.1088/1742-6596/2647/14/142009.

[10] Y. Zhang, Y. Miyamori, S. Mikami, et al. "Vibration-based structural state identification by a 1-dimensional convolutional neural network". In: *Structural Health Monitoring* 24.1 (2019), pp. 822–839.

[11] M. Jamshidi and M. El-Badry. “Structural damage severity classification from time-frequency acceleration data using convolutional neural networks”. In: *Structures* 54 (2023), pp. 236–246.

[12] C. Rinaldi et al. “Long-term vibrational monitoring of the Exedra of Marcus Aurelius’ Hall”. In: *Lecture Notes in Civil Engineering*. Vol. 305. 2024, pp. 183–194. DOI: 10.1007/978-3-031-61421-7_13.

[13] N.L. Pham, Q.B. Ta, and J.T. Kim. “CNN-based damage identification of submerged structure–foundation system using vibration data”. In: *Applied Sciences* 14.17 (2024), p. 7508. DOI: 10.3390/app14177508.

[14] M. Crognale, A. Talebi, and V. Gattulli. “Assessing the Exedra Hall Digital Twin with a Recorded Urban Blast”. In: *Lecture Notes in Civil Engineering* (2026). accepted.

[15] S.-Y. Kim and M. Mukhiddinov. “Data anomaly detection for structural health monitoring based on a convolutional neural network”. In: *Sensors* 23.20 (2023), p. 8525. DOI: 10.3390/s23208525.

[16] M. Zhao, A. Sadhu, and M. Capretz. “Multiclass anomaly detection in imbalanced structural health monitoring data using convolutional neural network”. In: *Journal of Infrastructure Preservation and Resilience* 3.1 (2022), p. 10.

[17] M. Crognale et al. “Developing and testing high-performance SHM sensors mounting low-noise MEMS accelerometers”. In: *Sensors* 24.8 (2024), p. 2435. DOI: 10.3390/s24082435.

[18] C. Wu and H. Hao. “Numerical simulation of structural response and damage to simultaneous ground shock and airblast loads”. In: *International Journal of Impact Engineering* 31.6 (2005), pp. 699–717.